GPCR Engineering Yields High-Resolution Structural Insights into β2-Adrenergic Receptor Function

Daniel M. Rosenbaum,[1]* Vadim Cherezov,[2]* Michael A. Hanson,[2] Søren G. F. Rasmussen,[1] Foon Sun Thian,[1] Tong Sun Kobilka,[1] Hee-Jung Choi,[1,3] Xiao-Jie Yao,[1] William I. Weis,[1,3] Raymond C. Stevens,[2]† Brian K. Kobilka[1]†

[1]Department of Molecular and Cellular Physiology, Stanford University School of Medicine, Stanford, CA 94305, USA. [2]Department of Molecular Biology, The Scripps Research Institute, La Jolla, CA 92037, USA. [3]Department of Structural Biology, Stanford University School of Medicine, Stanford, CA 94305, USA.

*These authors contributed equally to this work.

†To whom correspondence should be addressed. Email: stevens@scripps.edu (R.C.S.); kobilka@stanford.edu (B.K.K.)

The β2-adrenergic receptor (β2AR) is a well-studied prototype for G protein-coupled receptors (GPCRs) that respond to diffusible hormones and neurotransmitters. To overcome the structural flexibility of the β2AR and to facilitate its crystallization, we engineered a β2AR fusion protein in which T4 Lysozyme replaces most of the third intracellular loop of the GPCR ("β2AR-T4L"), and showed that this protein retains near-native pharmacologic properties. Analysis of adrenergic receptor ligand-binding mutants within the context of the reported high-resolution structure of β2AR-T4L provides insights into inverse agonist binding and structural changes required to accommodate catecholamine agonists. Amino acids known to regulate receptor function are linked through packing interactions and a network of hydrogen bonds, suggesting a conformational pathway from the ligand-binding pocket to regions that interact with G proteins.

The adrenergic receptors comprise a class of G protein-coupled receptors (GPCRs) that play a central role in mediating the effects of catecholamine hormones. In contrast to rhodopsin, which is expressed at very high levels in photoreceptor cells and has the ligand retinal covalently bound (1), other GPCRs such as the β2-adrenergic receptor (β2AR) generally express at low levels, bind diffusible ligands, and exhibit greater functional and structural plasticity (2). The β2AR was the first non-rhodopsin GPCR to be cloned, and has been one of the most extensively studied members of this large receptor family.

In order to obtain high-resolution structural information on the β2AR, we increased its proteolytic stability and crystallizability by eliminating the C-terminal tail and replacing most of the third intracellular loop (ICL3) with the protein T4 lysozyme (T4L). The optimized β2AR-T4L protein was crystallized in lipidic cubic phase, as described in the companion paper (3), and the resulting 2.4 Å resolution crystal structure reveals the interface between the receptor and the ligand carazolol, a partial inverse agonist (4). Analysis of mutagenesis data in light of the structure clarifies the roles of different amino acids in inverse agonist binding, and implies that rearrangement of the binding pocket accompanies agonist binding. In addition, the structure reveals how mutations known to cause constitutive activity or uncoupling of agonist binding and G-protein activation are distributed between the ligand-binding pocket and the cytoplasmic surface of the protein, such that changes in side chains due to interaction with the ligand can be transmitted through the structure to the site of G protein interaction.

β2AR-T4L: A crystallizable GPCR fusion protein. The conformational complexity that makes GPCRs versatile signaling molecules may contribute to the difficulty of crystallizing these proteins (2). Despite substantial efforts, we were unable to grow diffraction quality crystals from purified, homogeneous wild-type β2AR. This was likely due to conformational variability of the flexible ICL3 and carboxyl terminus, as well as the relatively small polar surface available for crystal contacts. Fluorescence resonance energy transfer experiments show that the carboxy-terminal portion of the β2AR is in an extended conformation (5), a property that may be important for the role of this region in interacting with signaling and scaffold proteins but which would likely interfere with crystal lattice formation. ICL3, which links the cytoplasmic ends of helices V and VI, is functionally important both for the specificity of receptor-G protein interactions and for G protein activation. In the β2AR this domain is susceptible to proteolysis; however, proteolytic cleavage does not lead to dissociation of the transmembrane segments linked by the ICL3. In fact, β2AR helices I-V and helices VI-VII behave as independent folding domains that can be expressed on separate plasmids and assemble to form a

functional "split" receptor (6). Therefore, we speculated that ICL3 links two domains with a relatively dynamic interface, which could be important for function but may also contribute to greater instability.

Since the majority of membrane protein crystals form through contacts of the non-membranous portions of the molecule, we sought to improve the chances of β_2AR crystallization by replacing ICL3 with a well-structured, soluble domain that might aid in the formation of lattice contacts. The initial criteria for choosing the inserted soluble protein were that the amino and carboxyl termini would approximate the predicted distance between the cytoplasmic ends of helix V and helix VI, and that the protein would crystallize under a variety of conditions. T4L is a small, stable protein that fulfills these criteria (7). The amino and carboxyl termini of wild-type T4L are 10.7 Å apart in PDB 2LZM (8), compared to a distance of 15.9 Å between the carboxyl carbon of residue $228^{5.63}$ (9) and the amide nitrogen of residue $241^{6.24}$ in the high-resolution structure of rhodopsin (PDB 1U19) (10).

DNA encoding the T4L protein (C54T, C97A) (11) was initially cloned into the human β_2AR gene, guided by comparison of ICL3 length and sequence among class A GPCRs (12): residues $234^{5.73}$- $259^{6.21}$ of the β_2AR were replaced by residues 2-164 of T4L (construct "E3" in Fig. 1A). In addition, the receptor was truncated at position 365, which aligns approximately with the position of the rhodopsin carboxyl terminus. Although these modifications resulted in a receptor that was expressed efficiently in Sf9 cells, further optimization was carried out to reduce the length of the junction between the receptor and the T4L termini (13). Several candidate constructs are illustrated in Fig. 1A, and selected immunofluorescence images of transfected, permeabilized HEK293 cells are shown in Fig. 1B. Relative to the initial construct, we could remove three residues from the cytoplasmic end of helix V, three residues from the C-terminal end of T4L, and three residues from the N terminus of helix VI, all without losing significant cell-surface expression. The final construct used for crystallization trials ("β_2AR -T4L") has residues $231^{5.70}$-$262^{6.24}$ of the β_2AR replaced by amino acids 2-161 of T4L ("1D" in Fig. 1A). Similar reduction of flexibility through minimization of linker length has been important in previous crystallization studies on soluble fusion proteins (14).

Functional properties of β_2AR-T4L. We measured saturation binding of [³H]DHA to the β_2AR-T4L, as well as competition binding of the inverse agonist ICI-118,551 and several agonists (Fig. 2A, fig. S1, and table S1). The results show that β_2AR-T4L has wild-type affinity for the antagonist [³H]DHA and the inverse agonist ICI-118,551, whereas the affinity for both agonists (isoproterenol, epinephrine, formoterol) and a partial agonist (salbutamol) is two to three-

fold higher relative to wild-type β_2AR. Higher agonist binding affinity is a property associated with constitutively active mutants (CAMs) of GPCRs. CAMs of the β_2AR also exhibit elevated basal, agonist-independent activation of Gs, and typically have lower expression levels and reduced stability (15, 16). β_2AR-T4L exhibits binding properties of a CAM, but it expresses at levels exceeding 1 mg per liter of Sf9 cell culture, is more resistant to trypsin proteolysis than the wild-type β_2AR (fig. S2), and retains binding activity in detergent at 37 °C as well as the wild-type receptor (fig. S3).

β_2AR-T4L did not couple to G_s, as expected due to the replacement of ICL3 by T4L. To assess whether the fused protein alters receptor function at the level of its ability to undergo conformational changes, we used a covalently attached fluorescent probe as a reporter for ligand-induced structural changes. Fluorophores attached at $Cys265^{6.27}$, at the cytoplasmic end of helix VI, detect agonist-induced conformational changes that correlate with the efficacy of the agonist towards G protein activation (17–20). Detergent-solubilized β_2AR365 (wild-type receptor truncated at 365) and β_2AR-T4L were each labeled with monobromobimane, which has been used previously to monitor conformational changes of the β_2AR (21). Addition of the agonist isoproterenol to purified β_2AR365 induces a decrease in fluorescence intensity and a shift in λ_{max} for the attached bimane probe (Fig. 2B and table S2). These changes in intensity and λ_{max} are consistent with an agonist-induced increase in polarity around bimane. A smaller change is observed with the partial agonist salbutamol, while the inverse agonist ICI-118,551 had little effect. For the β_2AR-T4L, there are subtle differences in the baseline spectrum of the bimane-labeled fusion protein, as might be expected if the environment around $Cys265^{6.27}$ is altered by T4L. However, the full agonist isoproterenol induces a qualitatively similar decrease in intensity and rightward shift in λ_{max}. Thus the presence of the fused T4L does not prevent agonist-induced conformational changes. The partial agonist salbutamol induced larger responses in β_2AR-T4L than were observed in wild-type β_2AR, and there was a small increase in fluorescence in response to the inverse agonist ICI-118,551. These are properties observed in CAMs (15, 22) and are consistent with the higher affinities for agonists and partial agonists exhibited by β_2AR-T4L. Therefore, we conclude that the T4L fusion induces a partial constitutively active phenotype in the β_2AR, likely caused by changes at the cytoplasmic ends of helices V and VI.

Comparison between β_2AR-T4L and β_2AR-Fab structures. The β_2AR-T4L fusion strategy is validated by comparison of its structure to the structure of wild-type β_2AR complexed with a Fab that recognizes a three dimensional epitope consisting of the amino and carboxyl-terminal ends of ICL3, determined at an anisotropic resolution of 3.4 Å/3.7 Å

(*23*). Figure 3A illustrates the similarity between the fusion and antibody complex approaches to β2AR crystallization, in that both strategies rely on attachment (covalent or non-covalent, respectively) of a soluble protein partner between helices V and VI. A major difference between the two structures is that the extracellular loops and the carazolol ligand could not be modeled in the β2AR-Fab complex, whereas these regions are resolved in the structure of β2AR-T4L. Nonetheless, it is clear that the T4L insertion does not significantly alter the receptor. Superposition of the two structures (fig. S4) illustrates that the transmembrane helices of the receptor components are very similar (RMSD = 0.8 Å for 154 common modeled transmembrane Cα positions, versus 2.3 Å between β2AR-T4L and the 154 equivalent residues in rhodopsin), especially when the modest resolution of the Fab complex is taken into account.

There is one significant difference between the Fab-complex and chimeric receptor structures that can be attributed to the presence of T4L. The cytoplasmic end of helix VI is pulled outward as a result of the fusion to the carboxyl terminus of T4L, which alters the packing of Phe264[6.26] at the end of helix VI (Fig. 3B). In the Fab-complex β2AR, interactions between Phe264[6.26] and residues in helix V, helix VI, and ICL2 may be important in maintaining the β2AR in the basal state. The loss of these packing interactions in β2AR-T4L could contribute to the higher agonist binding affinity characteristic of a CAM.

An unexpected difference between the structure of rhodopsin and the β2AR-T4L involves the sequence E/DRY found at the cytoplasmic end of helix III in 71% of class A GPCRs. In rhodopsin, Glu134[3.49] and Arg135[3.50] form a network of hydrogen bond and ionic interactions with Glu247[6.30] at the cytoplasmic end of helix VI. These interactions have been referred to as an "ionic lock" that stabilizes the inactive state of rhodopsin and other class A members (*24*). However, the arrangement of the homologous residues is significantly different in β2AR-T4L: Arg131[3.50] interacts primarily with Asp130[3.49] and a sulfate ion rather than with Glu268[6.30], and the distance between helix III and helix VI is greater than in rhodopsin (Fig. 3C). This difference might be explained by the interaction between Glu268[6.30] and Arg8 of T4L; however, the arrangement of Asp130[3.49] and Arg131[3.50] and the distance between helix III and helix VI is very similar to that observed in the β2AR-Fab structure. While the presence of an antibody or T4L at the ICL3 region could potentially affect the arrangement of these residues, the fact that similar ionic lock structures were obtained using two different approaches suggests that a broken ionic lock may be a genuine feature of the carazolol-bound state of the receptor.

Ligand binding to the β2AR. The β2AR-T4L fusion protein was purified and crystallized in complex with the inverse agonist carazolol. Carazolol stabilizes the β2AR against extremes of pH and temperature, perhaps related to its unusually high binding affinity ($K_d < 0.1$ nM) and slow dissociation kinetics ($t_{1/2} \sim 30$ h) (fig. S5). The interactions between carazolol and β2AR-T4L are depicted schematically in Fig. 4. The carbazole ring system is oriented roughly perpendicular to the plane of the membrane, and the alkylamine chain (atoms 15–22 in the model) is nearly parallel to the heterocycle (Fig. 5, A and B). Carazolol was modeled into the electron density (*3*) as the (S)-(-) isomer due to the higher affinity of this enantiomer, despite the fact that a racemic mixture of the ligand was used in crystallization. Asp113[3.32], Tyr316[7.43], and Asn312[7.39] present a constellation of polar functional groups to the alkylamine and alcohol moieties of the ligand, with Asp113[3.32] and Asn312[7.39] sidechains forming close contacts (<3Å) with O_{17} and N_{19} atoms of carazolol (Figs. 4 and 5, A and B). Asp113[3.32] was one of the first β2AR residues shown to be important for ligand binding; notably the D113N mutation causes complete loss of detectable affinity for antagonists (*25*) and a decrease in the potency of agonists towards cell-based G protein activation by over 4 orders of magnitude (*26*). Likewise, mutations of Asn312[7.39] perturb β2AR binding to agonists and antagonists: changes to nonpolar amino acids (Ala or Phe) reduce affinities to undetectable levels, while retention of a polar functionality (Thr or Gln) gives partial affinity (*27*). On the opposite end of the ligand near helix V, N_7 of the carbazole heterocycle forms a hydrogen bond with the side chain hydroxyl of Ser203[5.42]. Interestingly, mutations of Ser203[5.42] specifically decrease β2AR affinity towards catecholamine agonists and aryloxyalkylamine ligands with nitrogen-containing heterocycles such as pindolol (*28*), and by implication carazolol. Thus, the polar interactions between carazolol and the receptor observed in the crystal structure agree with the known biochemical data. The contribution of Tyr316[7.43] to antagonist and agonist affinity remains to be tested; this residue is conserved as tyrosine in all sequenced adrenergic receptor genes (*12*).

Figure 5C shows the tight packing between carazolol and surrounding amino acids that buries 790 Å^2 of surface area from solvent; specific contacts are depicted schematically in Fig. 4. Notable among the hydrophobic residues contacting carazolol are Val114[3.33], Phe290[6.52], and Phe193[5.32]. The side chain of Val114[3.33] from helix III makes multiple contacts with the C_8-C_{13} ring of the carbazole heterocycle, and Phe290[6.52] from helix VI forms an edge-to-face aromatic interaction with the same ring. As a result, these two amino acids form a hydrophobic "sandwich" with the portion of the aryl moiety that is common to many adrenergic antagonists. Mutation of Val114[3.33] to alanine was shown to decrease β2AR affinity towards the antagonist alprenolol by an order of magnitude, as well as lowering affinity for the agonist

epinephrine 300-fold (*29*). Phe193[5.32] is different from other carazolol contact residues in that it is located on the ECL2, in the path of hormone accessibility to the binding pocket. This amino acid contributes more buried surface area than any other residue to the interface between β_2AR-T4L and carazolol (see table S3). Therefore, Phe193[5.32] is likely to contribute significantly to the energy of β_2AR-carazolol complex formation, and the position of this residue on the extracellular side of the binding site may allow it to act as a gate that contributes to the unusually slow dissociation of the ligand (fig. S5).

Analysis of the binding pocket provides insights into the structural basis for pharmacologic selectivity between the β_2AR and closely related adrenergic receptors such as the β_1AR. The affinities of these two receptors for certain ligands, such as ICI-118,551, betaxolol and RO363 (*30*), differ by up to 100-fold. Curiously, all of the amino acids in the carazolol binding pocket are conserved between the β_1AR and β_2AR [see fig. S6 (*13*)]. The majority of the 94 amino acid differences between the β_1AR and β_2AR are found in the cytoplasmic and extracellular loops. While residues that differ in the transmembrane segments generally face the lipid bilayer, eight residues lie at the interface between helices and may influence helix packing. The structural basis for pharmacologic differences between β_1AR and β_2AR must, therefore, arise from amino acid differences in the entrance to the binding pocket or subtle differences in the packing of helices. Evidence for the latter comes from chimeric receptor studies (*31*) in which successive exchange of helices between β_1AR and β_2ARs led to a gradual change in affinity for the β_2AR selective ICI-118,551 and the β_1AR selective betaxolol.

As discussed above, β_2AR-T4L shows CAM-like properties with respect to agonist binding affinities, suggesting that the unliganded β_2AR-T4L may exist in a more active conformation than the wild type-β_2AR. Nevertheless, as shown in Fig. 2B, β_2AR-T4L can be stabilized in an inactive conformation by an inverse agonist. Since β_2AR-T4L was crystallized with bound carazolol, a partial inverse agonist, the structure most likely represents an inactive state. This is consistent with the similarity of the β_2AR-T4L and β_2AR-Fab5 carazolol-bound structures. To assess whether conformational changes are required to accommodate catecholamines, a model of isoproterenol was placed in the binding site such that common atoms (16–22 in Fig. 4) were superimposed onto the analogous carazolol coordinates in the crystal structure (Fig. 5D). Residues Ser204[5.43] and Ser207[5.46] are critical for catecholamine binding and activation of the β_2AR, with Ser204[5.43] hydrogen bonding to the meta-hydroxyl and Ser207[5.46] to the para-hydroxyl of the catechol ring, respectively (*32*). In our model, the catechol hydroxyls of isoproterenol face the appropriate serines on helix V, but the distances are too long for hydrogen bonding (6.8 Å from

meta-hydroxyl oxygen to the sidechain oxygen of Ser204[5.43], 4.8 Å from the para-hydroxyl oxygen to the sidechain oxygen of Ser207[5.46]). In addition, Asn293[6.55] and Tyr308[7.35], two residues expected to form selective interactions with agonists based on the literature (*33*, *34*), are too distant to form productive polar or hydrophobic contacts with the modeled isoproterenol molecule. These observations suggest that agonist binding requires changes in the binding site relative to the carazolol-bound structure, unless common structural components of agonists and inverse agonists bind in a significantly different manner.

Structural insights into β_2AR activation. Biophysical studies provide evidence that conformational changes associated with activation of the β_2AR are similar to those observed for rhodopsin (*2*, *18*, *21*, *35*). Yet the highly efficient process of light activation of rhodopsin through the *cis-trans* isomerization of covalently bound retinal is very different from activation of the β_2AR and other GPCRs by diffusible hormones and neurotransmitters (*2*). Despite representing a static picture of the inverse agonist-bound state, the crystal structure of β_2AR-T4L may still provide clues as to how agonist binding is translated into structural changes in the cytoplasmic domains of receptor. Agonist binding occurs at the extracellular ends of helices III, IV, V and VII, and G protein activation is mediated by the cytoplasmic ends. While the structure is open at the extracellular face to form the ligand binding pocket, the helices are more closely packed in the intracellular half of the receptor. This close packing implies that isolated rigid-body movement of any of these helices is unlikely, and that conformational changes can only be accomplished by rearrangement of side chains forming the network of interactions between the helices. Biophysical studies show that structurally different agonists stabilize distinct active states (*17*, *20*), suggesting that different ligands could stabilize different combinations of side chain rearrangements.

Analysis of mutations that affect β_2AR function provides insights into structural rearrangements that are likely to occur during receptor activation. Figure 6A illustrates the location of amino acids for which mutations lead to elevated basal, agonist-independent activity (constitutively active mutations, CAMs), as well as amino acids for which mutations impair agonist activation (uncoupling mutations, UCMs). Residues for which CAMs have been described are likely to be involved in interactions that maintain the receptor in the inactive conformation. These amino acids are centrally located on helices III and VI. In contrast, positions in which UCMs have been observed are likely to form intramolecular interactions that stabilize the active state. A cluster of UCMs are found at the cytoplasmic end of helix VII. Neither CAMs nor UCMs are directly involved in agonist binding. Although the CAMs and UCMs are not directly connected in sequence,

it is evident from the structure that they are linked through packing interactions, such that movements in one will likely affect the packing of others. For example, Fig. 6A (right panel) shows all amino acids with atoms within 4 Å of the two centrally located CAMs, Leu124$^{3.43}$ (*36*) and Leu272$^{6.34}$ (*37*). Several amino acids that pack against these CAMs also interact with one or more UCMs. Trp286$^{6.48}$ lies at the base of the binding pocket. It has been proposed that agonist binding leads to a change in the rotameric state of Trp286$^{6.48}$ with subsequent changes in the angle of the helical kink formed by Pro288$^{6.50}$ (*38*). It is likely that an agonist-induced change in the rotameric state of Trp286$^{6.48}$ will be linked to changes in sidechains of CAMs and UCMs through packing interactions and propagated to the cytoplasmic ends of the helices and the associated intracellular loops that interact with G proteins and other signaling molecules.

In the structures of both rhodopsin and the β$_2$AR, a cluster of water molecules lies near the most highly conserved class A GPCR residues (Fig. 6B). It has been proposed that these water molecules may play a role in the structural changes involved in receptor activation (*39*). Figure 6C shows the network of potential hydrogen bonding interactions that link Trp286$^{6.48}$ with conserved amino acids extending to the cytoplasmic ends of helices. UCMs have been identified for three amino acids linked by this network - N322$^{7.49}$, P323$^{7.50}$, and Y326$^{7.53}$ (*40*). This relatively loose-packed, water filled region is likely to be important in allowing conformational transitions, as there will be fewer steric restraints to sidechain repacking. Future structures of the agonist-bound state of the β$_2$AR will help to clarify the precise rearrangements that accompany activation of the receptor.

While crystallization of β$_2$AR-T4L in the presence of other ligands remains an exciting prospect, future efforts to obtain structures of the catecholamine-bound receptor will be challenging due to the relatively low affinity of these compounds in the absence of G protein, and their chemical lability. Moreover, biophysical studies indicate that agonist binding and activation is a multi-step process involving distinct conformational intermediates (*2*, *17*, *19–21*, *41*), which produces structural heterogeneity even at saturating concentrations of agonist. It is therefore possible that structural elucidation of the active state of the β$_2$AR will only be possible through crystallization of the complex between agonist, β$_2$AR and cognate G protein.

References and Notes

1. H. G. Khorana, *J. Biol. Chem.* **267**, 1 (1992).
2. B. K. Kobilka, X. Deupi, *Trends Pharmacol. Sci.* **28**, 397 (2007).
3. V. Cherezov *et al.*, *Science*, 25 October 2007 (10.1126/science.1150577).
4. The efficacy of a ligand describes the effect of the ligand on the functional properties of a GPCR. Agonists are defined as ligands that fully activate the receptor. Partial agonists induce submaximal activation even at saturating concentrations. Inverse agonists inhibit basal receptor activity. Antagonists have no effect on basal activity, but competitively block access of other ligands. Carazolol, is defined as a partial inverse agonist because it suppresses only 50% of the basal activity of the β$_2$AR.
5. S. Granier *et al.*, *J. Biol. Chem.* **282**, 13895 (2007).
6. B. K. Kobilka *et al.*, *Science* **240**, 1310 (1988).
7. X. J. Zhang, J. A. Wozniak, B. W. Matthews, *J. Mol. Biol.* **250**, 527 (1995).
8. L. H. Weaver, B. W. Matthews, *J. Mol. Biol.* **193**, 189 (1987).
9. Ballesteros-Weinstein numbering is used throughout the text as superscripts to the protein numbering. Within each helix is a single most conserved residue among the class A GPCRs. This residue is designated X.50, where x is the number of the transmembrane helix. All other residues on that helix are numbered relative to this conserved position.
10. T. Okada *et al.*, *J. Mol. Biol.* **342**, 571 (2004).
11. M. Matsumura, W. J. Becktel, M. Levitt, B. W. Matthews, *Proc. Natl. Acad. Sci. U.S.A.* **86**, 6562 (1989).
12. F. Horn *et al.*, *Nucleic Acids Res.* **31**, 294 (2003).
13. Materials and methods and supplementary figures are available as supporting material on *Science* Online.
14. D. R. Smyth, M. K. Mrozkiewicz, W. J. McGrath, P. Listwan, B. Kobe, *Protein Sci.* **12**, 1313 (2003).
15. U. Gether *et al.*, *J. Biol. Chem.* **272**, 2587 (1997).
16. S. G. Rasmussen *et al.*, *Mol. Pharmacol.* **56**, 175 (1999).
17. P. Ghanouni *et al.*, *J. Biol. Chem.* **276**, 24433 (2001).
18. P. Ghanouni, J. J. Steenhuis, D. L. Farrens, B. K. Kobilka, *Proc. Natl. Acad. Sci. U.S.A.* **98**, 5997 (2001).
19. G. Swaminath *et al.*, *J. Biol. Chem.* **279**, 686 (2004).
20. G. Swaminath *et al.*, *J. Biol. Chem.* **280**, 22165 (2005).
21. X. Yao *et al.*, *Nat. Chem. Biol.* **2**, 417 (2006).
22. P. Samama, S. Cotecchia, T. Costa, R. J. Lefkowitz, *J. Biol. Chem.* **268**, 4625 (1993).
23. S. G. Rasmussen *et al.*, *Nature*, published online 21 October 2007; 10.1038/nature06325.
24. J. A. Ballesteros *et al.*, *J. Biol. Chem.* **276**, 29171 (2001).
25. C. D. Strader *et al.*, *Proc. Natl. Acad. Sci. U.S.A.* **84**, 4384 (1987).
26. C. D. Strader *et al.*, *J. Biol. Chem.* **263**, 10267 (1988).
27. S. Suryanarayana, B. K. Kobilka, *Mol. Pharmacol.* **44**, 111 (1993).
28. G. Liapakis *et al.*, *J. Biol. Chem.* **275**, 37779 (2000).
29. P. Chelikani *et al.*, *Proc. Natl. Acad. Sci. U.S.A.* **104**, 7027 (2007).
30. Y. Sugimoto *et al.*, *J. Pharmacol. Exp. Ther.* **301**, 51 (2002).
31. T. Frielle, K. W. Daniel, M. G. Caron, R. J. Lefkowitz, *Proc. Natl. Acad. Sci. U.S.A.* **85**, 9494 (1988).

32. C. D. Strader, M. R. Candelore, W. S. Hill, I. S. Sigal, R. A. Dixon, *J. Biol. Chem.* **264**, 13572 (1989).

33. K. Wieland, H. M. Zuurmond, C. Krasel, A. P. Ijzerman, M. J. Lohse, *Proc. Natl. Acad. Sci. U.S.A.* **93**, 9276 (1996).

34. H. Kikkawa, M. Isogaya, T. Nagao, H. Kurose, *Mol. Pharmacol.* **53**, 128 (1998).

35. U. Gether *et al.*, *EMBO J.* **16**, 6737 (1997).

36. Y. X. Tao, A. N. Abell, X. Liu, K. Nakamura, D. L. Segaloff, *Mol. Endocrinol.* **14**, 1272 (2000).

37. A. D. Jensen *et al.*, *J. Biol. Chem.* **276**, 9279 (2001).

38. L. Shi *et al.*, *J. Biol. Chem.* **277**, 40989 (2002).

39. L. Pardo, X. Deupi, N. Dolker, M. L. Lopez-Rodriguez, M. Campillo, *Chembiochem* **8**, 19 (2007).

40. L. S. Barak, L. Menard, S. S. Ferguson, A. M. Colapietro, M. G. Caron, *Biochemistry* **34**, 15407 (1995).

41. M. J. Lohse, C. Hoffmann, V. O. Nikolaev, J. P. Vilardaga, M. Bunemann, *Adv. Protein Chem.* **74**, 167 (2007).

42. W. L. DeLano, The PyMOL Molecular Graphics System (2002) on the World Wide Web www.pymol.org.

43. A. W. Schuettelkopf, D. M. F. van Aalten, *Acta Crystallogr. D Biol. Crystallogr.* **D60**, 1355 (2004).

44. M. J. Zuscik, J. E. Porter, R. Gaivin, D. M. Perez, *J. Biol. Chem.* **273**, 3401 (1998).

45. F. Z. Chung, C. D. Wang, P. C. Potter, J. C. Venter, C. M. Fraser, *J. Biol. Chem.* **263**, 4052 (1988).

46. O. Moro, M. S. Shockley, J. Lameh, W. Sadee, *J. Biol. Chem.* **269**, 6651 (1994).

47. S. A. Green, G. Cole, M. Jacinto, M. Innis, S. B. Liggett, *J. Biol. Chem.* **268**, 23116 (1993).

48. A. M. Gabilondo *et al.*, *Proc. Natl. Acad. Sci. U.S.A.* **94**, 12285 (1997).

Supporting Online Material

Fig. 1. Design and optimization of the β₂AR-T4L fusion protein. (**A**) The sequence of the region of the β₂AR targeted for insertion of a crystallizable domain is shown, and the positions of the junctions between the receptor and T4L (in red) for various constructs are indicated. The sequences that were initially replaced or removed are faded. Red lines are shown after every tenth residue. (**B**) Immunofluorescence images of HEK293 cells expressing selected fusion constructs. Panels on the left shows M1 anti-FLAG signal corresponding to antibody bound to the N-terminus of the receptor. Panels on the right show the same signal merged with blue emission from DAPI (nuclear staining for all cells). Plasma membrane staining is observed in the positive control,

D3 and D1, while C3 and D5 are retained in the endoplasmic reticulum.

Fig. 2. Functional characterization of β_2AR-T4L. (**A**) Affinity competition curves for adrenergic ligands binding to β_2AR-T4L and wild-type β_2AR. Binding experiments on membranes isolated from Sf9 insect cells expressing the receptors were performed as described (*13*). (**B**) β_2AR-T4L is still able to undergo ligand-induced conformational changes. Bimane fluorescence spectra (excitation at 350 nm) of detergent-solubilized β_2AR-T4L and wild-type β_2AR truncated at 365, labeled under conditions that selectively modify $Cys265^{6.27}$ (*13*), were measured after incubating unliganded receptor with compounds for 15 min at room temperature. The cartoon illustrates that the observed changes in fluorescence can be interpreted as a movement of the bimane probe from a more buried, hydrophobic environment to a more polar, solvent-exposed position.
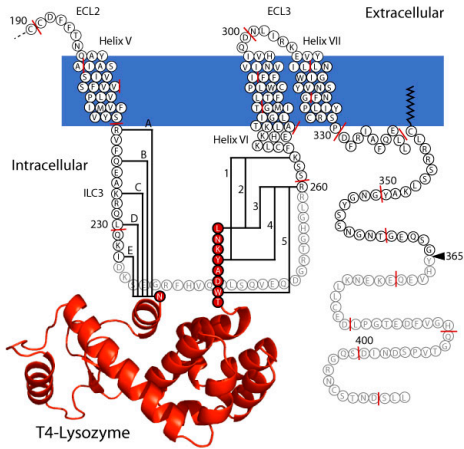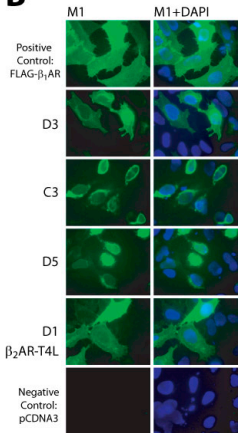
Fig. 3. (**A**) Side-by-side comparison of the crystal structures of the β_2AR-T4L fusion protein and the complex between β_2AR365 and a Fab fragment. The receptor component of the fusion protein is shown as a blue cartoon (with modeled carazolol as red spheres), while the receptor bound to Fab5 is in yellow. (**B**) Differences in the environment surrounding $Phe264^{6.26}$ (shown as spheres) for the two proteins. (**C**) The analogous interactions to the "ionic lock" between the E(D)RY motif and $Glu247^{6.30}$ seen in rhodopsin (right panel, purple) are broken in both structures of the β_2AR (left panel, colored blue and yellow as above). Pymol (*42*) was used for the preparation of all figures.

Fig. 4. Schematic representation of the interactions between β_2AR-T4L and carazolol at the ligand binding pocket. Residues shown have at least one atom within 4 Å of the ligand in the 2.4 Å resolution crystal structure.
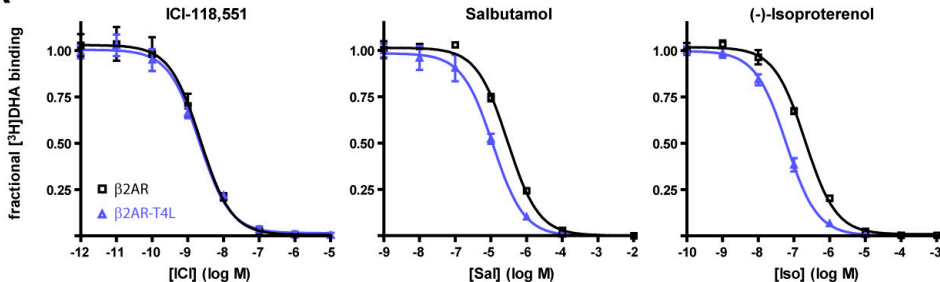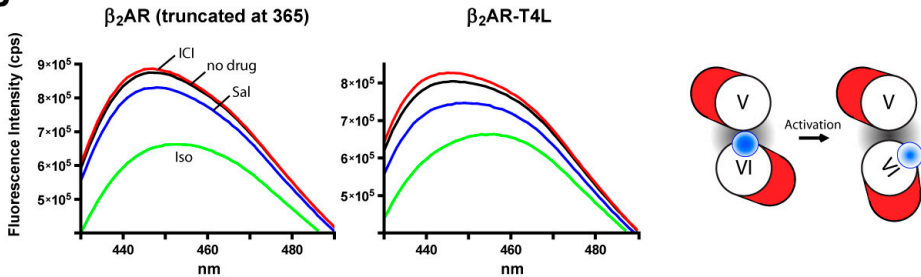
Fig. 5. The ligand binding pocket of β_2AR-T4L with carazolol bound. (**A**) Residues within 4 Å of the ligand are shown as sticks, with the exception of A200, N293, F289, and Y308. Residues that form polar contacts with the ligand (distance cutoff 3.5 Å) are in green, other residues are gray (in all panels, oxygens are colored red and nitrogens are blue). (**B**) Same as panel A, except that the ligand is oriented with its amine facing out of the page. W109 is not shown. (**C**) Packing interactions between carazolol and all residues within 5 Å of the ligand. View is from the extracellular side of the membrane. Carazolol is shown as yellow spheres, receptor residues are shown as sticks within van der Waals dot surfaces. $Val114^{3.33}$, $Phe193^{5.32}$, and $Phe290^{6.52}$ are colored red, all other residues are gray. (**D**) Model of (-)-isoproterenol (magenta sticks) in the ligand binding pocket observed in the crystal structure. A model of the agonist with optimal bond lengths and angles was obtained from the PRODRG server (*43*), and the dihedral angles were adjusted
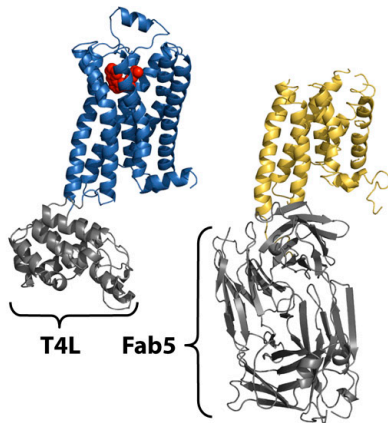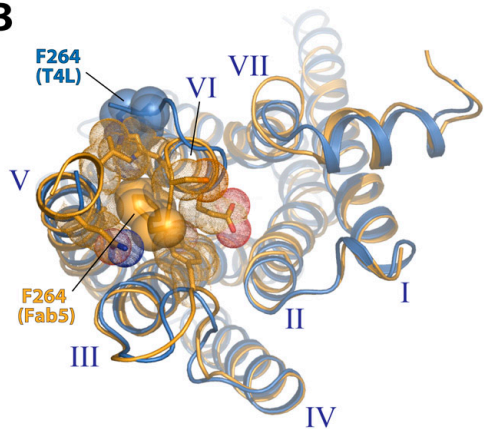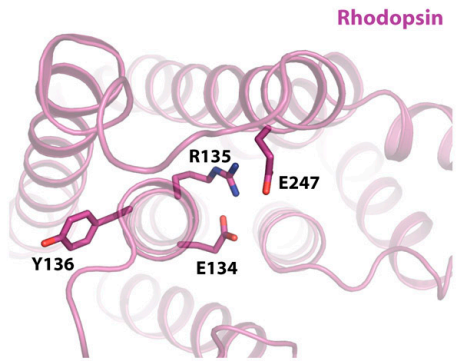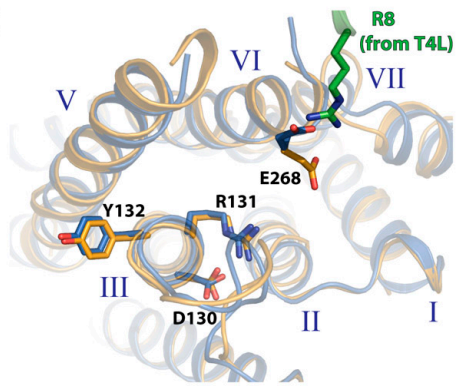
to the values observed in the homologous atoms of bound carazolol (16–22 in Fig. 4). The one remaining unaccounted dihedral in (-)-isoproterenol was adjusted in order to place the catechol ring in the same plane as the C_{16}-C_{15}-O_{14} plane in carazolol. Residues known to specifically interact with agonists are shown as green sticks.
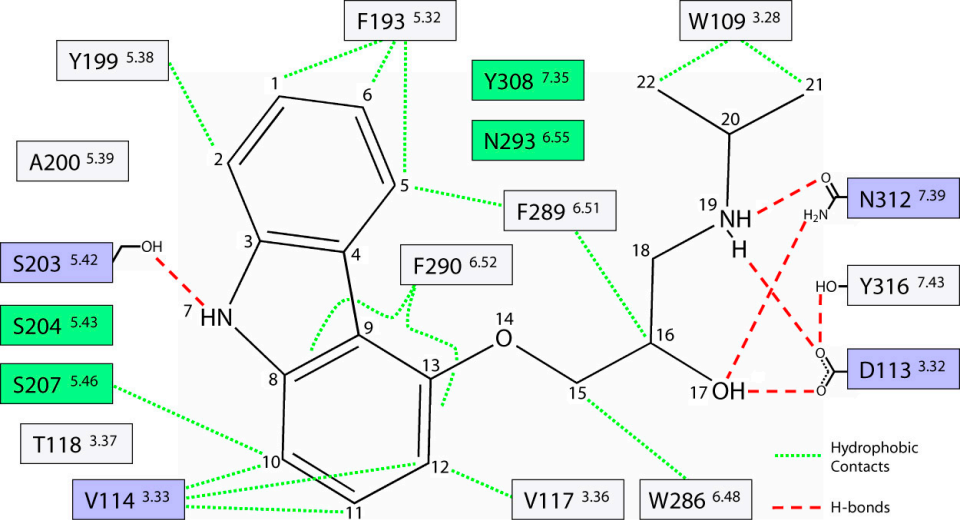
Fig. 6. Packing interactions in the β_2AR that are likely to be modulated during the activation process. (**A**) On the left, residues previously demonstrated to be CAMs (*16*, *24*, 36–*38*, *44*) or UCMs (*25*, *40*, *45*–*48*) are shown as van der Waals spheres mapped onto a backbone cartoon of the β_2AR-T4L structure. On the right, residues that are found within 4Å of the CAMs $Leu124^{3.43}$ and $Leu272^{6.34}$ are shown as yellow spheres or dot surfaces. A vertical cross-section through the structure illustrates that these surrounding residues connect the CAMs on helices III and VI with the UCMs on helix VII through packing interactions. (**B**) In both β_2AR-T4L (blue) and rhodopsin (purple), a network of ordered water molecules is found at the interface between the transmembrane helices at their cytoplasmic ends. (**C**) Network of hydrogen bonding interactions between water molecules and β_2AR-T4L residues (sidechains as blue sticks), notably the UCMs on helix VII (orange cartoon).

A

ECL2
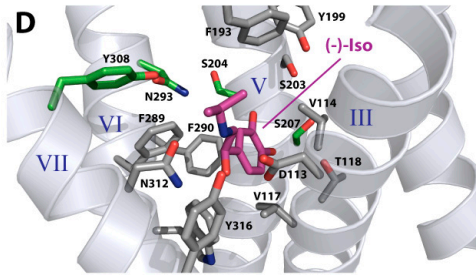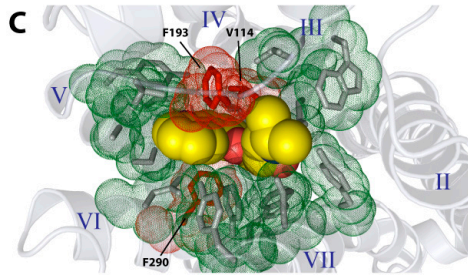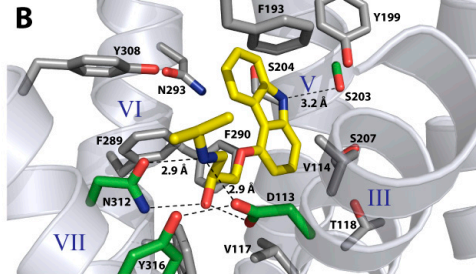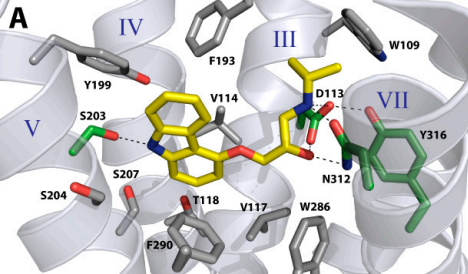190
Helix V
ECL3
300
Helix VII
Extracellular

Intracellular
Helix VI
ILC3
230
260
350
365
400
T4-Lysozyme

B

	M1	M1+DAPI
Positive Control: FLAG-β₁AR		
D3		
C3		
D5		
D1 β₂AR-T4L		
Negative Control: pCDNA3		

- Y199 5.38
- F193 5.32
- W109 3.28
- Y308 7.35
- N293 6.55
- A200 5.39
- F289 6.51
- N312 7.39
- S203 5.42
- F290 6.52
- Y316 7.43
- S204 5.43
- D113 3.32
- S207 5.46
- T118 3.37
- V114 3.33
- V117 3.36
- W286 6.48

········· Hydrophobic Contacts

- - - - - H-bonds

▨ Mutation disrupts antagonist and agonist binding

▨ Mutation disrupts agonist binding

A

VI
VII
W286
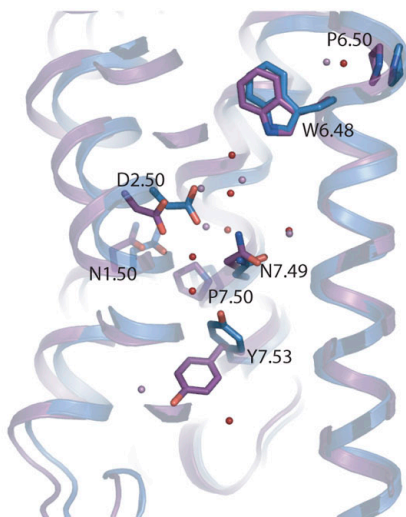III
V
L124
L272

UCMs - green spheres
CAMs - red spheres

B

Rhodopsin water ⬤   **β₂AR** water ⬤

P6.50
W6.48
D2.50
N1.50   N7.49
P7.50
Y7.53

C

III   I   VII
II   VI
G7.42   W6.48
S7.46   N7.45
D2.50   F7.48
N1.50   I6.40
N7.49
I2.43   Y7.53